Received: 25 May 2020 | Revised: 7 October 2020 | Accepted: 16 November 2020

DOI: 10.1002/eqe.3401

WILEY

RESEARCH ARTICLE

Multihazard framework for investigating high-rise base-isolated buildings under earthquakes and long-duration winds

Tathagata Roy[1] | **Taiki Saito**[1] | **Vasant Matsagar**[2]

[1] Research Center for Collaborative Area Risk Management (CARM), Department of Architecture and Civil Engineering, Toyohashi University of Technology, Toyohashi, Japan

[2] Multihazard Protective Structures (MHPS) Laboratory, Department of Civil Engineering, Indian Institute of Technology (IIT) Delhi, New Delhi, India

Correspondence
Taiki Saito, Research Center for Collaborative Area Risk Management (CARM), Department of Architecture and Civil Engineering, Toyohashi University of Technology (TUT), 1-1 Hibariga-oka, Tempaku-cho, Toyohashi, Aichi - 441-8580, Japan.
Email: tsaito@ace.tut.ac.jp

Abstract

Japan experiences a considerable number of low to medium earthquake shocks and long-duration winds throughout the year, which is relatively more as compared to other different regions of the world. Considering this multihazard scenario, structures designed using the existing guidelines may have significant chances to underestimate the induced distress level in the structure as well as in the energy dissipation devices, which are designed based on traditional peak variables neglecting accumulation of damage. To overcome the shortcoming of the existing assessment technique, a multihazard framework is formulated that deals in estimating probable number of earthquakes and long-duration winds likely to occur in the design life of a structure. The sequence of design earthquakes and long-duration winds obtained through the proposed methodology is subsequently implemented in base-isolated high-rise buildings of two different heights, which are designed based on Japanese standard. Responses are addressed in terms of displacement and acceleration at isolation and top floor level, force-deformation and fatigue damage induced in the isolation devices under individual and multihazard scenarios. Results show that a particular range of building exists that is governed by both earthquake and wind events, and it is recommended that design of such building types should include the effects of both hazards. Moreover, the series of events likely to occur in design life of the buildings induce significant damage in the isolators as compared to the individual hazard event, thereby emphasizing a strong need to develop multihazard framework, where the occurrence rate of such extreme events is relatively higher.

KEYWORDS

base isolation, earthquake, fatigue, high-rise building, multihazard, wind

1 | INTRODUCTION

In recent years, increase in urbanization has led to the construction of larger number of high-rise buildings in Japan, and in this regard, the extent of danger posed by the occurrence of huge numbers of earthquake and wind events in this region cannot be overlooked. To minimize the damaging effects under these natural hazards, base-isolation devices have been in use to enhance the performance of structure and infrastructure systems, especially, under the earthquakes,[1–5] and

nowadays under the winds.[6,7] The base-isolation systems are recognized to be one of the most effective techniques in limiting the amount of damage in superstructure for low- to mid-rise buildings due to a substantial amount of period lengthening. However, in high-rise buildings that have long periods, the effectiveness of the isolation systems is observed to be limited, as the shift in the fundamental period is relatively lesser. Nevertheless, considering other beneficial aspects such as habitability (occupant comfort) and functionality restoration (no damage to structural and nonstructural components), the base-isolation systems have also emerged to be one of the attractive solutions for the newly constructed high-rises against the earthquake and wind loadings.[8,9] Practical applications of the base-isolation systems are also observed in high-rise buildings, such as the Sendai MT building at Sendai, Japan (85 m), Nakanoshima Festival Tower at Osaka, Japan (200 m), Shimizu Corporation Tokyo Headquarters at Tokyo, Japan (100 m), etc. Thus, the effectiveness of isolation systems installed in high-rise buildings is not completely ruled out, wherein the isolation devices installed in such high-rise building scenario needs to be thoroughly investigated under the effects of multiple earthquakes and wind hazards.

The use of base-isolation devices in high-rise buildings is widely recognized in Japan, where more than 20% of the super-high-rise buildings are base-isolated, and more than 80% of the base-isolated buildings are condominium in the Osaka city of Japan.[10] Yet, utilization of this advanced technique is uncommon in most parts of the world,[11] and as a result, research has not been fully explored to investigate the performance of the isolation devices in high-rise buildings under earthquakes and winds. Initially, Ariga et al[12] investigated the behavior of base-isolated high-rise buildings under long-period ground motions. They concluded that friction-type bearings are effective in avoiding the resonance of the structure with ground motions. Roussis and Constantinou[13] investigated the use of isolation devices in high-rise buildings that can potentially lead to overturning of the superstructure by attracting large tensile stresses in the isolation system. Takewaki[14] investigated the robustness of base-isolated high-rise buildings under code-specified ground motions. It was concluded that the base-isolation devices used in high-rise buildings had relatively lower robustness as compared to base-isolated low-rise buildings. Ma et al[15] obtained seismic responses of base-isolated high-rise buildings in stochastic domain subjected to fully nonstationary earthquake ground motions. Nakai et al[16] evaluated stiffness of the base-isolation layer of a high-rise isolated building as well as the stiffness of superstructure using the earthquake response observation records under different amplitude levels. They concluded that with increase in the amplitude, the superstructure encountered a reduction in stiffness, which confirmed the amplitude dependence of the stiffness of superstructure. Lately, research has also been focused in proposing new isolation techniques to overcome the overturning hazard induced in the isolation devices.[17,18]

Base-isolated high-rise buildings are more susceptible to wind loads in comparison to the fixed-base high-rises, as the wind excitations favor structures with relatively reduced modal frequency.[19] Although, base-isolation devices are generally designed for earthquake loads, the effectiveness under wind loads in such high-rises currently demands more attention. Initial studies focused on estimating the response parameters for structures that are governed by wind loadings.[20,21] Thereafter, Yasui et al[22] proposed analytical methods to determine wind responses of base-isolated high-rise buildings with creep phenomena. Higashino et al[23] conducted fatigue tests on sliding bearings, especially for the rubber pad, at each wind level that the building experiences during its lifetime. They observed that the fatigue demand was at par with the expected fatigue level for the lifetime of a structure equipped with base-isolation system. Katagiri et al[24] investigated the along-wind, across-wind, and torsional responses of base-isolated high-rise buildings. They concluded that unstable aerodynamic response could be observed in across-wind and torsional directions in lightly weighted base-isolated high-rise buildings. Recently, Li et al[25] studied the wind-resistant design of base-isolated high-rise buildings including the design of isolation system and the modeling of equivalent static wind load (ESWL). They concluded that the variation in isolation layer can increase the additional stiffness and damping, and subsequently can suppress responses.

To summarize, the investigations in the field of base-isolated high-rise buildings under earthquakes and winds merely focused on the traditional design parameters of the buildings in terms of peak drift, displacement, acceleration, shear force, and similar response quantities. As most of the regions in Japan experience low to medium earthquakes and long-duration annual winds throughout the year, occurrence of such multiple events during design life of the structure may inflict more damage in the isolation systems due to excessive accumulation of energy. In this case, the isolation systems may succumb to fatigue failure. In this context, the Japan Society of Seismic Isolation (JSSI) manual stated that if a seismically isolated building, especially lead rubber bearing (LRB), is exposed to a long-duration strong wind, internal temperature rises and the change in hysteretic characteristics of the device is of significant concern.[26] The JSSI manual also stressed the necessity to assess the long-duration high-cycle fatigue damage in the isolation system for several strong winds that may occur in the design life of a base-isolated building. Moreover, few researches demonstrated that the failure is significantly more for high-rise structures installed with different passive control dampers under multihazard (MH) scenario of high-amplitude earthquake and high-cycle wind.[27,28] Based on these facts, the performance of any energy-dissipating device

TABLE 1 Target performance for base-isolated buildings[31]

Events	Level 1	Level 2
Performance	**Damage limitation**	**Life safety**
Superstructure	Interstorey drift < 1/500	Interstorey drift < 1/300
Base-isolation device	Shear strain, γ < 100-150%	Shear strain, γ < 150-250% Tensile stress < 1 MPa
Substructure	Storey drift < 1/1000	Storey drift < 1/500

(here, isolation systems) in terms of fatigue behavior requires intensive investigation under the sequence of low to severe earthquake motions and long-duration wind loadings, as the frequency of occurrence of such events are significantly higher in Japan.[29]

Herein, base-isolated high-rise reinforced concrete (RC) buildings having 20 and 25 storeys are investigated under individual earthquake and wind scenarios, and subsequently compared against the proposed multi-hazard (MH) scenario. The isolation devices considered here are LRBs. The base-isolated high-rises including the LRBs are modeled in a finite element (FE) software package (STructural Earthquake Response Analysis 3D [STERA_3D]) considering nonlinearities in the model. The responses are addressed in terms of displacement and acceleration at isolation and top floor level, and force-deformation and fatigue response in the isolation devices under individual design level earthquake and wind. Therefore, based on the above-mentioned research gaps, the objectives outlined for the current study are: (a) to develop an MH framework for determining probable number of earthquake and wind events likely to occur in design life of structures; (b) to investigate the performance of the 20- and 25-storey base-isolated high-rise buildings under a set of individual earthquake and wind events, and further compare with the MH scenario; (c) to construct fatigue curve using the Manson-Coffin relation[30] for the considered LRBs under high-cycle loading to observe the failure of the LRBs; and (d) to estimate the fatigue life of the LRBs under the considered MH scenario of earthquakes and winds.

2 | DESIGN OF BASE-ISOLATION SYSTEM FOR HIGH-RISE BUILDING

The most recent building code provisions in Japan were introduced in 2000, where relevant guidelines were prescribed to design base-isolated buildings.[31] The guidelines recommended by the Japanese code are relatively clear regarding design of high-rises with isolation devices. On the contrary, the recommendations prescribed in other design codes, especially in the American standard, make the adoption of isolation systems difficult for high-rise buildings.[11] The use of base-isolation systems in Japan has been for more than couple of decades, wherein the target design requires enhanced performance as compared to the general structural design. The design of base isolation systems generally follows equivalent linearized method (ELM) for building with total height of less than 60 m. For buildings with more than 60 m height, time history analysis (THA) under design earthquake ground motions scaled to the hazard level is required to be used for obtaining the design requirements of the isolation systems.[32] As the present study involves performance evaluation of base-isolated high-rise buildings having height more than 60 m, the THA method is used to obtain the design specifications of the base-isolation devices, which is LRB.

The preliminary approach aims to design the isolator mainly using tributary gravitational loads, wherein the nominal long-term compressive stress of the isolators should be within the acceptable design limit. The limiting value for the nominal long-term compressive stress varies for different sizes of LRBs, where practical values range from 6 to 15 MPa, according to Bridgestone Corporation[33] (Bridgestone Corporation is one of the major organizations for manufacturing of seismic isolation devices in Japan). Here, nominal long-term compressive stress is referred as long-term upper limit or maximum limit of compressive stress induced in the isolators.[33] After choosing a particular set of LRB, the base-isolated high-rises are analyzed and designed using the guidelines recommended by the JSSI.[32] The manual recommends a two-level design procedure, wherein the base-isolated structure must satisfy the performance under two earthquake hazard levels. Level 1 corresponds to a 50-year return period, where the structure is checked for "damage limitation" performance and Level 2 corresponds to a 500-year return period earthquake, where the structure is designed for "life safety" performance. The details of the performance level against the hazard levels are presented in Table 1. In addition to the above-mentioned criteria, pull-out resistance of the isolators against the vertical force must be checked and should be within the allowable tensile stress limit, as the isolators tend to induce large tensile forces under the dynamic loadings, which result in uplifting and overturning of the base-isolated building. In this regard, the allowable tensile stress at 100% strain level is adopted as 1 MPa.

TABLE 2 Characteristics of lead rubber bearings (LRBs) used in 20- and 25-storey high-rise reinforced concrete (RC) buildings

Specification	20-storey (LH100G4)	25-storey (LH110G4)
First and second shape factor	37.3/4.98	37.2/5.51
Diameter and rubber height (mm)	1000/201	1100/201
Device height and lead plug diameter (mm)	400.6/150	390.2/170
Initial and postyield stiffness (kN/mm)	19.8/1.52	24.1/1.85
Characteristic strength (kN)	141	181
Design deformation (mm)	402	402

Considering these criteria, the designed base-isolated high-rise building is checked against the prescribed levels of ground motions. In case the prescribed performance is not satisfied, an iterative approach is subsequently used to ensure the superstructure satisfies the performance criteria under the above-mentioned hazard levels. Following the above-mentioned design philosophy, the 20-storey high-rise building is designed for LRB having lead plug diameter of 150 mm and total rubber thickness of 200 mm, whereas the 25-storey high-rise is designed for LRB having lead plug diameter of 170 mm and total rubber thickness of 200 mm. The other fundamental design variables for the LRBs are presented in Table 2.

3 | MODELING AND ANALYSIS OF BASE-ISOLATED HIGH-RISE BUILDINGS

3.1 | Structural description

The 20- and 25-storey base-isolated high-rise buildings are assumed to be located in Toyohashi city of Aichi prefecture in Japan. The target high-rise buildings are RC structures, each having an isolation layer in the basement. The design of the base-isolated high-rise buildings is in accordance with the Japanese standard, wherein the designed isolation devices are chosen from the catalogue provided by the Bridgestone company. The base-isolated high-rise buildings are designed for earthquakes using time-history analysis, as the building heights are more than 60 m. The superstructure is checked for storey drift <1/300 under the "Level 2" earthquakes that correspond to 500-year return period. The height of the isolation floor is designed to be 2.2 m, whereas height of each storey is considered to be 3.5 m as shown in Figure 1. The details of the superstructure, including the design details of beams and columns for the 20- and 25-storey base-isolated high-rise RC buildings are presented in Tables 3 and 4. The seismic isolation devices installed in both the high-rise buildings are the LRBs. The ultimate shear strain of the LRBs is 400%, whereas the LRBs in serviceable conditions are allowed to deform up to 200%.

3.2 | Numerical model and analysis

Plane frame models of the 20- and 25-storey base-isolated high-rise RC buildings are developed and analyzed by STERA_3D,[34] considering material and geometric nonlinearities. Beams of the superstructure are modeled using beam elements. Each beam element comprises of nonlinear flexural/bending springs at the two ends of the element and a nonlinear shear spring in the middle of the element. The hysteresis model for the bending springs of the beams is based on the Takeda Model, which involves degrading trilinear slip model to account for the difference in flexural capacity between positive and negative side of the beam, as shown in Figure 2. The hysteresis model of the nonlinear shear spring is defined by shear force and rotation that utilizes an origin-oriented polylinear model. The reinforcing steel strength is assumed to be 1.1 times larger than the nominal strength. The effective width of slab (S_b) that contributes for the flexural behavior of a beam is 0.1 L_b, where, L_b is the length of the beam. The stiffness degradation ratio in the trilinear Takeda model is considered to be 0.5, whereas the strength degradation is assumed to be 0.1. The ultimate rotation angle for the beam is considered as 1/50. The stiffness ratio in postyielding stage of the hysteresis model is assumed to be 0.001.

The column element is represented by multispring (MS) model, as shown in Figure 3, with nonlinear vertical springs at both ends and two-directional nonlinear shear springs in the middle of the element. The nonlinear bending spring at

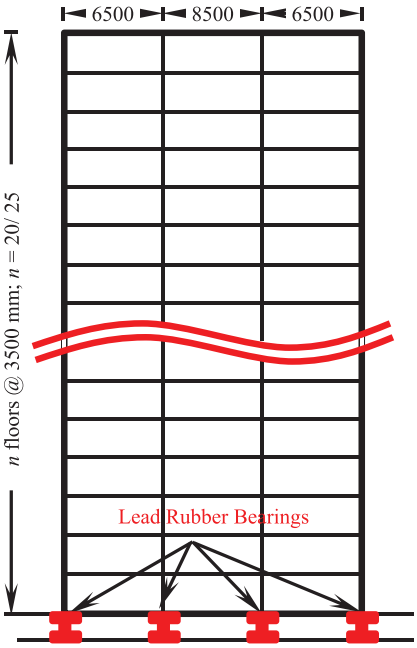

FIGURE 1 Elevation of the base-isolated high-rise building

TABLE 3 Details of beams and columns for 20-storey base-isolated high-rise building

Location	Size (mm)	Reinforcement		Material strength (MPa)
		Main (RM)	Shear (RS)	
Beam				
Isolator level	750 × 1200 Cover: 50	Top: 7-29 φ Bottom: 10-29 φ	4-13 φ@120 c/c	Concrete: 35 RM: 345 RS: 295
1F-5F	800 × 900 Cover: 50	Top: 9-32 φ Bottom: 12-32 φ		
6F-10F	750 × 900 Cover: 40	Top: 8-29 φ Bottom: 10-29 φ		
11F-15F	750 × 850 Cover: 40	Top: 7-29 φ Bottom: 10-29 φ	4-13 φ@150 c/c	
16F-20F	650 × 750 Cover: 40	Top: 7-29 φ Bottom: 10-29 φ		
Column				
1F-5F	1000 × 1000 Cover: 60	12-32 φ	4-13 φ@100 c/c	Concrete: 35 RM: 345 RS: 295
6F-10F	850 × 850 Cover: 60	12-29 φ		
11F-15F	800 × 800 Cover: 50	8-25 φ		
16F-20F	750 × 750 Cover: 50			

the member end is constructed from the nonlinear vertical springs that consider nonlinear interaction among moments and axial force, that is M_x-M_y-P_z. The section is divided in five zones, wherein, four corner zones have concrete and steel springs and the central area has one concrete spring (Figure 3). There are two nonlinear shear springs in X and Y directions. Hysteresis model of the nonlinear shear springs is the same as that considered in the beam element. The beam-column connection is idealized as a rigid zone, in which the default length of the rigid zone is set to be a half of the column

TABLE 4 Details of beams and columns for 25-storey base-isolated high-rise building

Location	Size (mm)	Reinforcement		Material strength (MPa)
		Main (RM)	Shear (RS)	
Beam				
Isolator level	1000 × 1400 Cover: 60	Top: 10-29 φ Bottom: 12-29 φ	4-13 φ@120 c/c	Concrete: 35 RM: 345 RS: 295
1F-5F	900 × 900 Cover: 60	Top: 15-32 φ Bottom: 15-32 φ		
6F-10F	850 × 900 Cover: 60	Top: 12-32 φ Bottom: 12-32 φ		
11F-15F	800 × 850 Cover: 50	Top: 15-29 φ Bottom: 15-29 φ	4-12 φ@120 c/c	
16F-20F	750 × 800 Cover: 50	Top: 12-29 φ Bottom: 12-29 φ	3-13 φ@150 c/c	
21F-25F	700 × 700 Cover: 40	Top: 10-29 φ Bottom: 10-29 φ		
Column				
1F-5F	1100 × 1100 Cover: 60	12-32 φ	4-13 φ@100 c/c	Concrete: 40 RM: 345 RS: 295
6F-10F	900 × 900 Cover: 60	12-29 φ		
11F-15F	850 × 850 Cover: 60	12-25 φ		
16F-20F	800 × 800 Cover: 60			
21F-25F	750 × 750 Cover: 50	10-20 φ	4-10 φ@100 c/c	

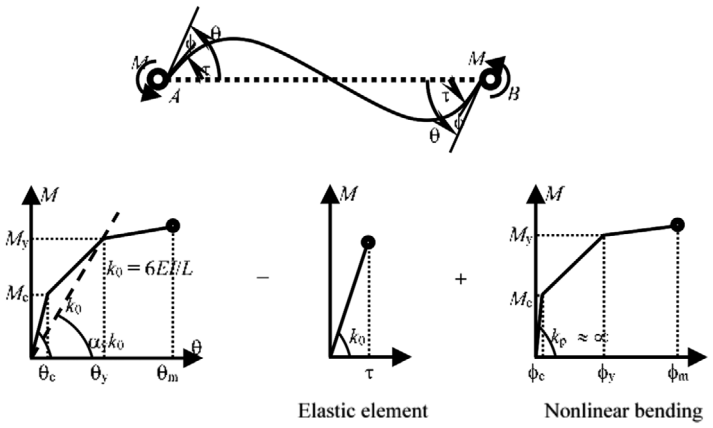

FIGURE 2 Moment-rotation relationship for bending spring

width, and the nonlinear bending spring of the beam element is arranged at the position of the column face. The floor slab is assumed to be elastic for in-plane deformation and free for out-of-plane deformation. P-delta effect is considered in element stiffness matrix of column. The seismic weights of the isolation layer (B1) and each floor of the superstructure are, respectively, obtained to be 2500 and 2000 kN.

The element model of the LRB consists of shear springs that are arranged in *x-y* plane, with change in direction having equal angle interval. This model, implemented in STERA_3D,[34] is known as multishear spring model (MSS), in which the hysteresis is defined as a bilinear model having initial and postyield stiffness, and yield shear force. The hysteresis model is modified in such a way that the hysteresis of LRB has stiffness degradation according to strain level. The LRB is susceptible to degradation due to increase in temperature developed from prolonged cyclic stress reversals[35–37]; hence,

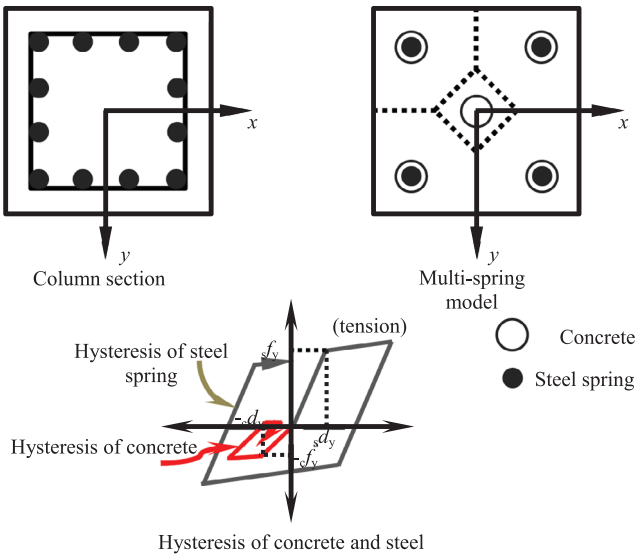

FIGURE 3 Multispring model for column and force-deformation curves for concrete and steel springs

the temperature-dependent effect in stiffness and yield shear force is taken into account. The reduction in strength of LRB results in deteriorating force-deformation characteristics for LRB, which is quite crucial for obtaining response of the base-isolated high-rises.[38–40] In this study, reduction in strength is considered from the dissipated energy through a reduction factor, which depends on the energy dissipated and volume of lead plug, although the isolator strength almost remains the same or slightly increases after the bearing has been subjected to a large number of cycles.[39–41] Further, there has been decrease in vertical stiffness of the LRB on application of lateral loading[42]; however, the magnitude of decrease is not significant, which is also captured in the MSS model used in this study. Also, the current study assumes that the bearing loses a part of its original strength after staying idle long enough, allowing the lead core temperature to drop, and the model used here considers strength reduction by dissipated energy.[34] The assumption in modeling of LRB is supported by the evidences that LRBs installed in bridges suffered extensive damage including rupture and cracking during the 2011 Great East Japan earthquake[43] and deterioration was observed in the LRBs after 10 years of service life.[44,45] In this regard, strength recovery is not considered in the current model of LRB. This is contradictory, given that the strength of an LRB recovers when the bearing is given some idle time that allows its lead core to cool down.[46] Moreover, the considered model does not account for cavitation. Hence, these aspects of modeling strategy may be considered as limitations of the present research conducted.

The numerical integration technique used to solve the system of equations is the unconditionally stable Newmark-β method. Each time step of input ground acceleration data is divided from 20 to 50 based on the type of loading to achieve relatively more accurate responses. Finally, the STERA_3D v10.3[34] program is modified to introduce a unique option for performing the sequence of analysis by developing a batch file that is linked with the source code of STERA_3D. By using such technique, it is ensured that a large number of multiple simulations are conducted without the interference of user.

4 | FRAMEWORK FOR ESTIMATING MULTIPLE EARTHQUAKE AND WIND EVENTS DURING DESIGN LIFE OF A STRUCTURE

Existing research in earthquake engineering utilizes probabilistic seismic hazard analysis (PSHA) technique for deriving seismic hazard models that considers spatial and temporal uncertainty in the model.[47] Using this concept, various seismic hazard models in terms of seismic risks were developed by different researchers. Atkinson et al[48] used power law for obtaining the average annual number of exceedances of a shock amplitude. Erel et al[49] used exponential function to calculate the annual probability of occurrence of an earthquake having specific intensity. Cornell and Merz[50] and Kiureghian and Ang[51] used earthquake magnitude to calculate cumulative distribution function (CDF) for occurrence of earthquake. More recently, the concepts of uniform hazard spectra (UHS) and mean conditional spectra are used nowadays to model earthquake hazard at a particular location.[47,52,53] Because temporal uncertainty of an earthquake is considered from the

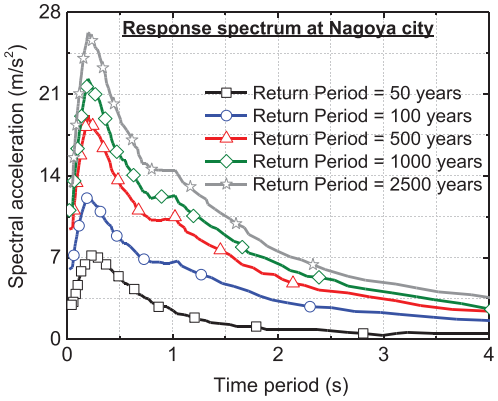

FIGURE 4 Earthquake response spectrum at Nagoya City

distribution of earthquake occurrences with respect to time, hence, the occurrence of an earthquake in a particular time interval was modeled as a Poisson process with the assumption that each event is independent in nature.[54] The Poisson process is considered to be the simplest and most widely used model for obtaining rate of occurrence of earthquakes exceeding certain intensity.[54–56] On the other hand, the wind hazard is represented by wind speed, which is direct function of the turbulence and frequency, or otherwise known as the spectral density or wind spectrum of the region. Most common spectrums used in wind engineering are von Karman spectrum and Kaimal spectrum depending on the turbulence of a region. To date, research has been progressing on estimating structural performance with the assumption that the structure is expected to resist maximum seismic force or maximum wind gust speed expected to occur once in the lifetime. However, it is evident that no such timeline has been proposed to date that utilizes multiple numbers of earthquakes based on return periods. In this regard, multiple earthquakes and winds are generated using their recurrence periods based on the assumption that the natural hazards are independent in nature and their recurrence follow Poisson point process. This traditional concept is used to generate a timeline of earthquake and wind occurrence, following the steps described in the sections below.

4.1 | Probability of earthquake or wind intensity

Let $n(i)$ and $t(i)$, respectively, be the average annual rate of occurrence and average return period for earthquake (e) or wind (w) with intensity more than i. Hence, the relation between annual occurrence rate and return period is used, which is given as

$$n\left(i=e,w\right)=1/t\left(i=e,w\right). \tag{1}$$

As the annual rate of occurrence for earthquake is $n(i=e)$, then according to the Gutenberg-Richter relationship, earthquake events having intensity i satisfies the following relationship[57,58]

$$\ln n=a-bi, \tag{2}$$

where, a is a constant and b is scaling parameter. Here, the earthquake intensity is considered to be the peak ground acceleration (PGA). In this case, the parameters, a and b are obtained from two sets of the intensity i and the return period t using Figure 4.

Now, assuming i_0 as the minimum intensity level considered, the CDF for the earthquakes with more than the intensity i (probability that i is less than or equal to j) is given as

$$F_e\left(j\right)=P\left(i<j\right)=1-N\left(j\right)/N_0, \tag{3}$$

where, $N_0=N(i_0)$.

TABLE 5 Parameters of probabilistic distribution of earthquake and wind intensity for Nagoya city

Event	Intensity, I	Return period (years)	Minimum intensity, I_0	Parameters
Earthquake	3 m/s^2	50	3 m/s^2	$a_e = -3.308$
	6 m/s^2	100		$b_e = 0.00216$
	11.05 m/s^2	1000		
	13.03 m/s^2	2500		
Wind	18 m/s	1	15 m/s	$a_w = 2.572$
	32 m/s	100		$b_w = 0.143$
	36 m/s	500		

In this study, the response spectrum is chosen for the Nagoya city, which is ~80 km from Toyohashi city. The details of the response spectrum are obtained from the Architectural Institute of Japan (AIJ) standard (Figure 4), which provides different levels of seismic hazard for the location.[52] The UHS technique, as provided in the AIJ[52] standard, is used to construct each level of seismic hazard having return periods of 50, 100, 500, 1000, and 2500 years. The PGA of an earthquake is considered as the spectral value at zero-period of the spectrum. Using this information, the parameters a and b to define the probabilistic occurrence of earthquake intensity are obtained using the above-mentioned relations.

The AIJ[52] classifies the wind loads based on recurrence period, such as: (a) weak and moderate winds, with frequent daily occurrence; (b) strong winds with 1-year return period; (c) rare winds with 50-year return period; and (d) extremely rare winds with 500-year return period. The basic wind speed (return period of 100 years) for Nagoya city is 32 m/s, whereas mean wind speeds having 1-year and 500-year return period are, respectively, estimated to be 18 and 36 m/s.[52] Further, the intensity of wind in terms of the average/mean speed of the Nagoya city for the past 50 years shows that the wind data set follows generalized extreme value distribution with ~15 m/s as mean wind speed. Therefore, the parameters for the wind hazard as well as the intensity curve are similarly estimated using the above-mentioned relations, wherein the intensity of wind is chosen to be the mean wind speed. Finally, Table 5 shows the parameters a and b obtained for the earthquake and wind intensity for Nagoya city. The minimum intensity levels considered in this study are 3 m/s^2 for earthquake and 15 m/s for wind.

4.2 | Probability of occurrence for earthquake or wind

Occurrence of every earthquake or wind event is independent, and such events follow a unique occurrence rate. As $n(i = e,w)$ is the average occurrence rate for the earthquake or wind events occur individually, then the probability of k earthquake or wind events of intensity more than i occurring in T-years can be expressed using Poisson process, which is given as

$$P_k(T) = [n(i)T]^k \frac{\exp[-n(i)T]}{k!}. \tag{4}$$

The probability of more than one earthquake or wind event exceeding intensity i in T years can be determined as

$$P(T) = 1 - P_0(T) = 1 - \exp[-n(i = e,w)T]^k. \tag{5}$$

It is regarded as the probability distribution of time interval t for the earthquake or wind event with intensity i.

4.3 | Generation of earthquake or wind events in design life of a building

The earthquake or wind events for a particular design or service period is generated using previous two steps, which links the probability of intensity and return period of the chosen hazards. The methodology involves generation of random samples from both sets that follow uniform distribution ∈ [0,1]. Here, the probability of occurrence for intensity is initially sampled, where $F_{e,w} \in [0,1]$, which is subsequently used to obtain the intensity $i(e,w)$ from the CDF plots that

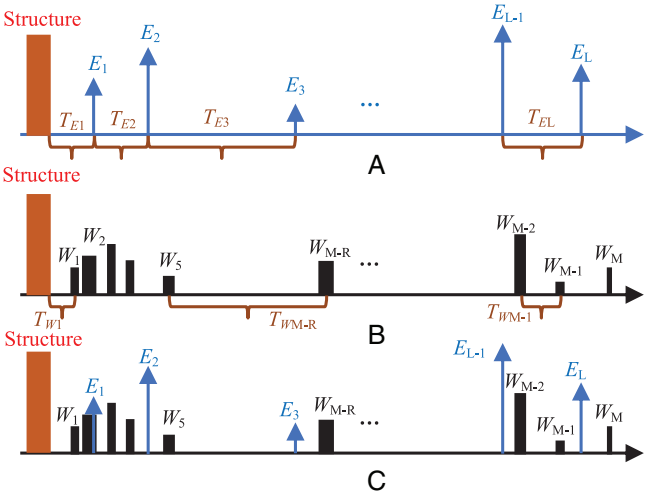

FIGURE 5 Generating timeline for earthquake and wind during design life of a structure

correspond to the random $F_{e,w}$. Likewise, each random number, sampled using uniform distribution from [0,1], which corresponds to the probability of recurrence period (obtained using step 4.2). Thereafter, the return period of each event, given by ${}_pt_q$, is obtained corresponding to the probability of occurrence. Finally, a set of L events with different intensities $i_p(p = 1, 2, 3, \ldots, L)$, with interval ${}_pt_q$ is arranged on the timeline. Considering the natural hazards, earthquake having intensity E and wind having intensity W, likely to occur in a region affecting the design of structure in the service life, two timelines are generated as shown in Figure 5A,B. Most importantly, the earthquake and wind events are assumed to occur independently, which allows to add the two timelines for obtaining the expected number of events in the design life of the building, which is shown in Figure 5C.

Finally, the steps for generating the events with different probabilities of exceedance are carefully delineated in the flowchart shown in Figure 6. For the present study, the design period is considered to be 100 years for investigating the base-isolated high-rise buildings, and five random set of timelines, shown in Figure 7, are generated to study the effectiveness of the base-isolation devices in the high-rise buildings.

Each realization of event has a unique probability weight associated, obtained from the uniform distribution, that allows for investigating the failure of the structure under each event. In this regard, Figure 8 is shown to present the probability weight of each event for the intensity of earthquake and wind events generated for the design life.

5 | EARTHQUAKE AND WIND HAZARDS

5.1 | Generation of spectrum-compatible ground motions

According to the current research standard,[31] response of important civil structures, such as base-isolated high-rise buildings, require relatively more careful analysis under ground motion excitations. In this regard, dynamic THA is recommended to be used for investigating these structures, and additionally the ground motion excitations should be scaled appropriately to fit the design response spectra available for a particular region. This technique is known as generation of spectrum-compatible earthquakes. Until now, many researches have been attempted to generate spectrum-compatible ground motions[59,60]; however, the present study utilizes Fourier transform technique, which is required to simulate nonstationary earthquake ground motion excitations that follows the response spectrum.[61] STERA_WAVE[61] is used to generate the spectrum-compatible ground motions using past-recorded motions. The use of this tool is just a choice, and comparison with other spectrum-compatible tools is not carried out.

The THA of the base-isolated high-rise buildings is conducted for each event of the timeline by generating the time history of each ground motion acceleration using Fourier spectrum and phase spectrum from the sample of earthquake intensity i (Figure 7) and the associated acceleration response spectrum given at the Nagoya site (Figure 4). The Fourier spectrum is calculated to be compatible to the target acceleration response spectrum. In this study, broadly two types of phase spectrums are used, namely, phase spectrum of historical ground motions and random phase. The phase

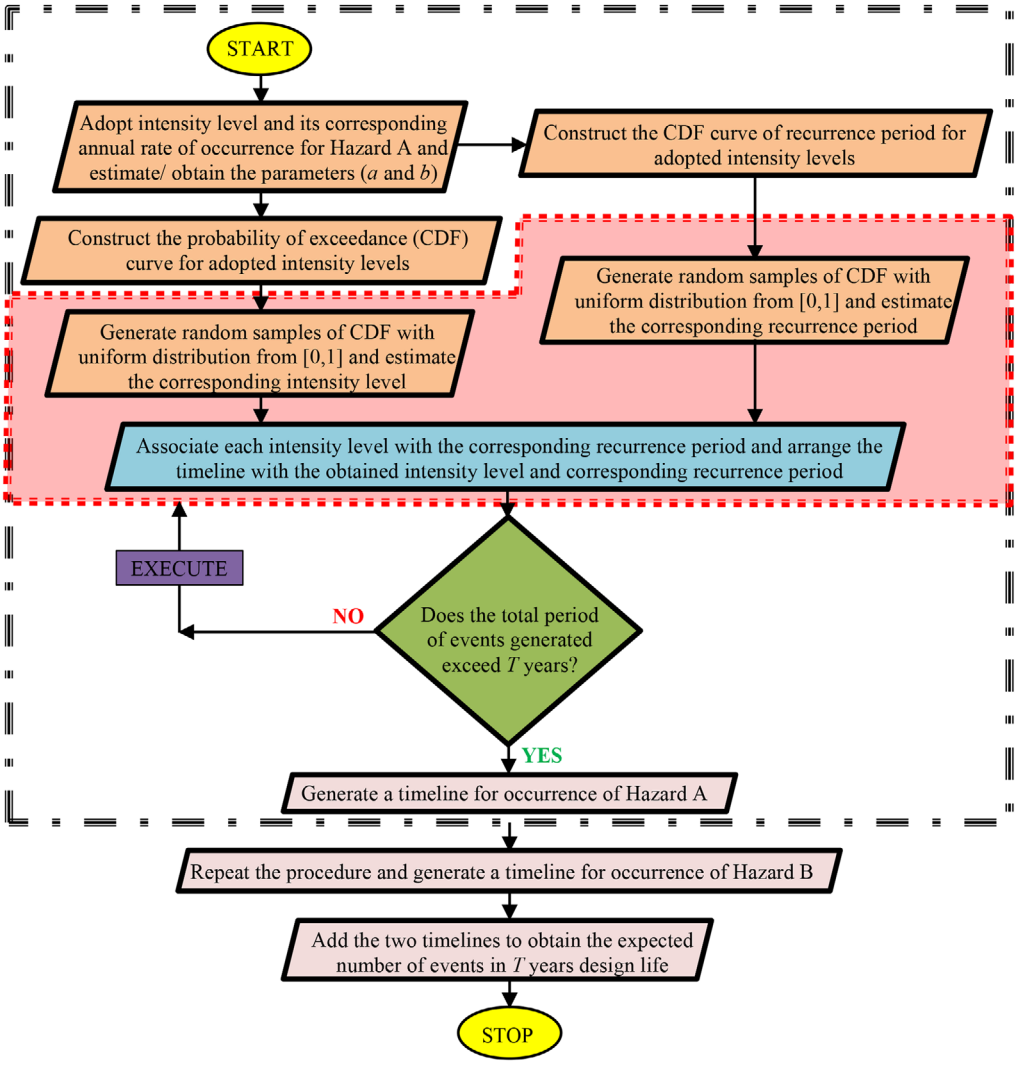

FIGURE 6 Framework for generating earthquake and wind during design life of a structure

spectra used here are chosen from the historical earthquakes that occurred in Japan, which are obtained from the Japan Meteorological Agency (JMA) database. The list of the historical ground motions used for all the presented timeline sets is shown in Table 6. For random phase, envelope function proposed by Jennings et al[62] is used to multiply a stationary time history. Table 7 shows the sequences of the phase spectrum earthquakes used in the timeline cases corresponding to Figure 7.

5.2 | Generation of long-duration wind loads

According to the JMA,[63] Japan experiences more than 24 typhoons or strong winds that strike every year, and more interestingly, the central Tokai region, that is, the region of interest experiences on an average of more than three typhoons of larger magnitude per year. It is also noteworthy to see that the duration of these strong winds in Japan is substantially higher[26] than the annual winds occurring in different parts of the world, which has more chances to induce high-cycle fatigue in any energy absorbing device installed in the civil structures. The JSSI[26] reports that the equivalent storm duration recorded at Tokyo and Kobe meteorological stations from 1997 to 2008 was from 30 minutes to more than 300 minutes. Hence, the impact of long-duration winds requires proper redressal to understand critical behavior, such as high-cycle fatigue in the energy-absorbing devices as well as the global performance of the structure, where the stress reversals are significantly greater.

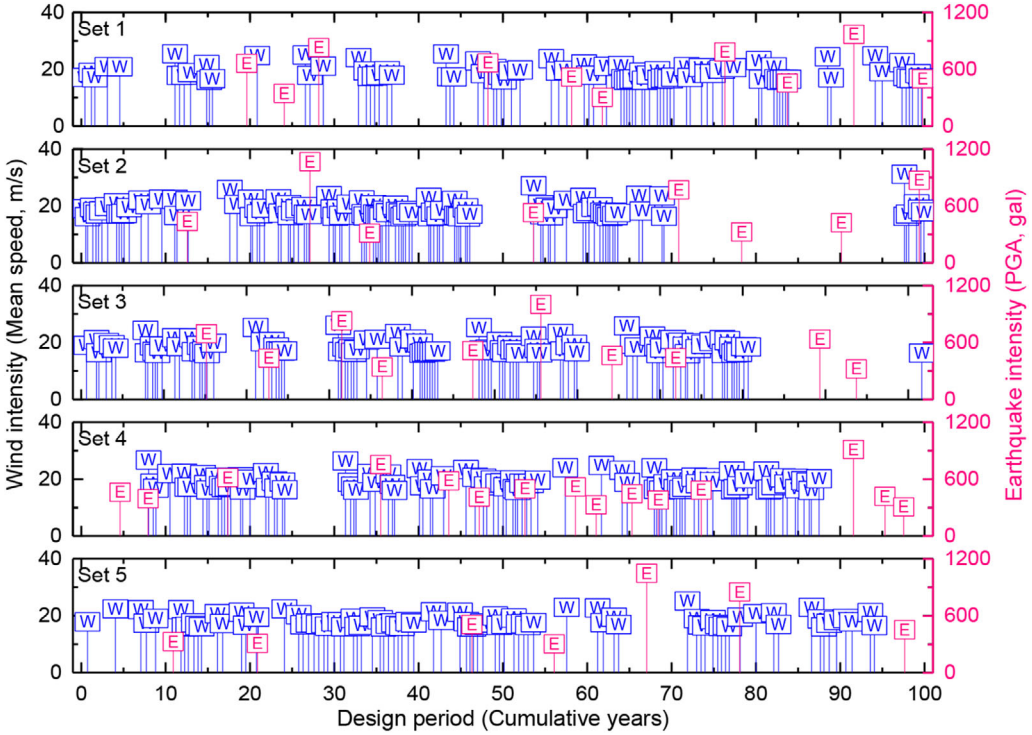

FIGURE 7 Timelines of earthquakes and winds generated through the proposed methodology

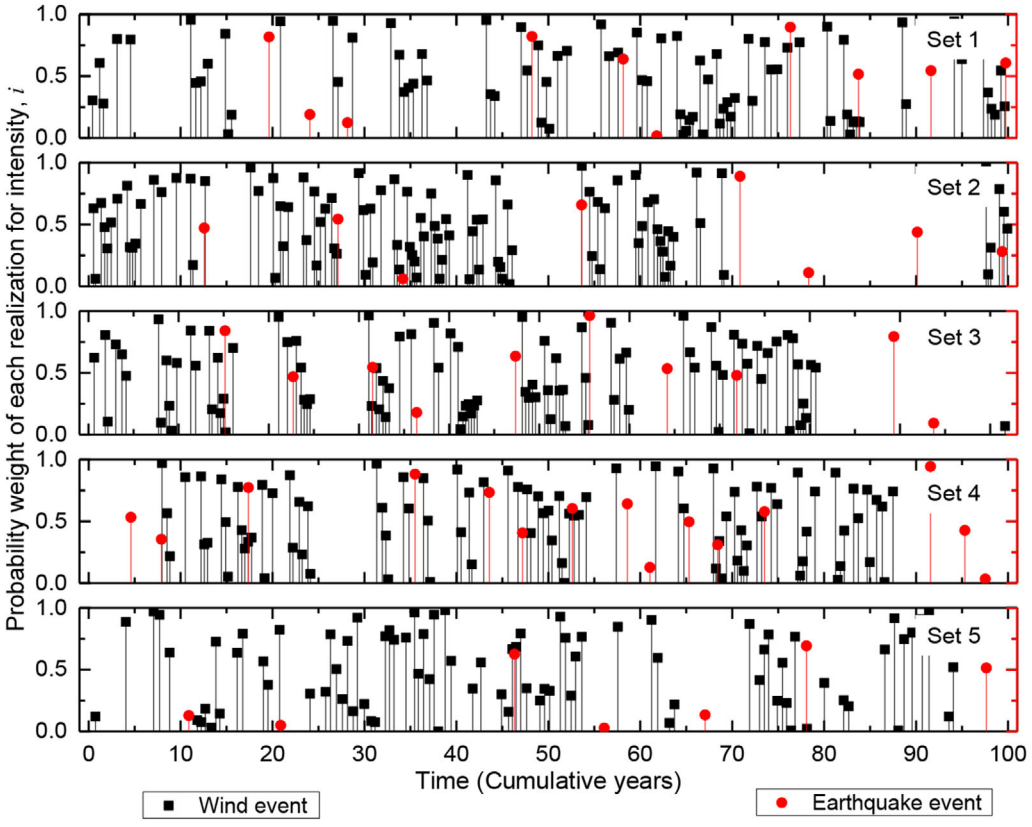

FIGURE 8 Probability weights of each realization for generated earthquake and wind events

TABLE 6 List of the historical ground motions used in the study

Sl. No.	Phase spectrum	Component	Date of occurrence	Recording station	Recorded PGA (m/s^2)	Duration (s)
1.	Random phase	–	–	–		120
2.	Kushiro Oki	NS	January 15, 1993	Kushiro	8.14	360
3.	Toho-Oki	NS	October 4, 1994	Honamachi	4.54	360
4.	Kobe	NS	January 17, 1995	JMA	8.18	60
5.	Tottori	NS	October 6, 2000	Yonago city	2.80	300
6.	Miyagi	EW	May 26, 2003	Izumimachi	6.55	120
7.	Tokachi-Oki	NS	September 26, 2003	Makuhetsu-cho	7.54	120
8.	Niigata-Chuetsu	NS	October 23, 2004	Ojiya city Castle	7.79	120
9.	Noto Hanto	NS	March 25, 2007	Wajima city	4.63	120
10.	Tohoku	EW	March 11, 2011	Ofunato	9.44	240
11.	Tottori	EW	October 21, 2016	Kurayoshi city	2.85	60
12.	Osaka	NS	June 18, 2018	Hirakata city	6.90	240
13.	Iburi	NS	September 6, 2018	Atsuma Kananuma	6.62	300
14.	Kumamoto	NS	January 3, 2019	Wadamachi Eda	2.62	60
15.	Yamagata	EW	June 18, 2019	Murakami city	11.84	60

TABLE 7 Sequence of the phase spectrum earthquakes used for multihazard analysis

Set No.	Sequence in timeline													
1.	7	5		15		8	9	1	4		2	10		12
2.	2		10		5		9	6		1		3		4
3.	8	3		4		5	12	10	2		9	7		1
4.	13	14	6	4	8	12	9	1	2	11	15	10	3	5
5.	3		1		12			5		10		4		13

The long-duration wind load comprises of static and fluctuating components, where the static component is described by the mean wind speed (U) and the fluctuating component (u) is described by the turbulence component in the atmospheric wind. The fluctuating component of the wind load is modeled for unidirectional case based on the von Karman spectrum provided in the AIJ.[52] The basic parameters, that is, the frequency spectrum of the wind load (f), the standard deviation (σ_u), and turbulence length (L_z) of fluctuating component of wind load are appropriately calculated from AIJ[52] based on the obtained mean wind speed, topography of location, and height of the high-rise buildings. The spatial correlation of wind speed along the height of the buildings is considered in terms of coherence function, given as

$$\gamma\left(f,d_j\right)=\frac{Re\left[S_{i_1,i_2}\left(f,d_j\right)\right]}{\sqrt{S_{i_1}\left(f\right)\cdot S_{i_2}\left(f\right)}}=\exp\left(-C_{ij}\frac{fd_j}{\bar{U}\left(z\right)}\right),i=u,v,w;j=v,w \tag{6}$$

$$\gamma\left(f,d_j\right)=\exp\left(-\frac{\sqrt{\left(C_{uy}\cdot fd_y\right)^2+\left(C_{uz}\cdot fd_z\right)^2}}{\bar{U}\left(z\right)}\right). \tag{7}$$

where, d_j is the distance between two nodes (here, storey height), S_u is single-point power spectral density of the turbulence for x-component. The decay coefficient C_{ij} is adopted from Norwegian Public Roads Administration Handbook N400[64]; whereas, power law is used to compute the wind speed for each Euclidian distance or storey level. Finally, conventional spectral representation method is used to simulate the multivariate random process in time domain to

obtain the fluctuating component of the wind load.[65,66] From Figure 7, each realization of wind in the timelines is a mean wind speed that is used to convert to wind time history by choosing appropriate parameters of fluctuating wind speed (eg, turbulence length, standard deviation, and duration). Since each set of timeline consists of 80-100 realizations for wind, in that case the standard deviation and duration parameters of fluctuating wind speed are obtained from a pool of random numbers that follows normal distribution. The mean for the duration and standard deviation of the wind load are adopted as 120 minutes and 6.73 m/s, with coefficient of variation (CoV) as 10% for both the parameters. It is to be noted that there is no specific guideline regarding the duration to be considered for analysis, and also there is no study that demonstrates the CoV for duration as well as standard deviation of the fluctuating component of wind.

6 | HIGH-CYCLE FATIGUE ESTIMATION OF LRB

The characteristics of earthquake or wind load, that is, high amplitude with low duration or low amplitude with high duration altogether have the possibility to induce different degrees of stress cycle in any energy-dissipating device (here, LRB). The higher number of cycles induces small elastic strains, which in turn initiates fatigue cracks on the surface of the material in these devices; as a result, the contribution of fatigue in the structural performance becomes noteworthy and cannot be ignored under the MH scenario. The importance to consider the fatigue behavior can also be observed from the damaged buildings caused by the recent devastating Tohoku-Pacific Ocean earthquake in 2011. A study was conducted by Kouchiyama et al[41] to assess the damaged buildings, and they demonstrated that the cracks generated in the damaged isolation devices were due to accumulation of energy under small-amplitude loading like middle-small earthquakes or winds, and not due to high-amplitude earthquakes for which the buildings are generally designed for. In this regard, the importance of cumulative energy dissipation in terms of fatigue response must be addressed to determine the safety of the buildings,[40] especially with energy-absorbing passive control devices under frequent medium earthquakes and long-duration wind loadings.

The fatigue response is generally determined using an *s-N* curve, where *s* is the stress amplitude, and *N* is the number of cycles until failure, wherein the stress amplitude may have constant or varying amplitudes. However, for the present study, constant amplitude load is used to determine the fatigue capacity in the form of *s-N* curve, which is otherwise termed as fatigue curve. Typical expression of the *s-N* curve or fatigue curve is approximated by a straight line where log *s* is plotted against log *N*, which is given in the form[30]

$$N = Cs^{-m}\ , \tag{8}$$

where, C and m are constants depending on the type of material. Here, equivalent deformation amplitude (δ) is used instead of stress amplitude.[67] It is to be noted that very limited research is available that presents the test results of LRB under low-amplitude high-cycle load.[26,40,41] Finally, a detailed step is presented below for obtaining the fatigue curve of the LRBs installed in the 20- and 25-storey base-isolated buildings.

6.1 | Steps for constructing fatigue curve of LRB under high-cycle loading

It is very important to understand the significance of the fatigue curve, which otherwise denotes the fatigue capacity of any energy-dissipating device, here LRB. The fatigue signifies the cumulative energy dissipation capacity of any device; hence, it is crucial to identify the limiting criteria for cumulative energy dissipation of the LRBs. Recent study published in the JSSI[68] manual provides the allowable energy dissipated by the lead core of the LRBs, which is 6.6 N-m/mm^3, required to compute the threshold fatigue limit. The value is obtained from experimental investigation that used a sequence of random cyclic and earthquake events to estimate the capacity for the LRB. In this regard, the corresponding fatigue capacity is calculated as 4×10^4 and 5×10^4 kN m, respectively, for each LRB installed in the 20- and 25-storey base-isolated buildings. The following points are finally outlined to clearly explain the procedure to construct the fatigue curve for the LRB under high-cycle loading.

1. Generate the fluctuating components of wind history (all storey levels), and having different standard deviations, for example, 2-10 m/s and loading durations,for example, 30 minutes to 10 hours. Here, wind history is used because of two important reasons: long duration and nearly constant amplitude. Moreover, different magnitudes of standard deviation

should provide different levels of amplitude, whereas different loading durations should help in obtaining the larger number of cycles.
2. Analyze the 20-storey base-isolated building under the generated load having a particular duration, and obtain the force-deformation response of the LRB. Compute the cumulative energy dissipation (demand) from the force-deformation response and the equivalent deformation amplitude (δ), which is defined as peak-to-peak deformation.
3. Check whether the demand response reaches or exceeds the capacity, which is 4×10^4 kN m. Calculate the number of cycles (N_f) until this threshold value, and plot the coordinate for δ and N_f.
4. Repeat the procedure for different amplitudes of wind load and different durations until sufficient number of points for δ and N_f are achieved.
5. Plot the fatigue curve in log-log scale and estimate a best-fit curve with least error.
6. Repeat the procedure for the 25-storey base-isolated building.

In this case, the Manson-Coffin empirical relations obtained based on the deformation amplitude, δ and the failure cycles N_f are given as

$$\delta_{\mathrm{LRB20}} = 25079 N_f^{-0.52}, \tag{9}$$

$$\delta_{\mathrm{LRB25}} = 28134 N_f^{-0.54}. \tag{10}$$

7 | NUMERICAL STUDY: INDIVIDUAL AND MULTIHAZARD SCENARIO

Herein, two cases of numerical study are conducted for the 20- and 25-storey base-isolated high-rises; one is for individual hazard (IH) scenario and another is MH timeline scenario. As discussed above, the responses under the IH scenarios may be underestimated that may have the potential to inflict damage in the LRBs. Hence, the responses considering the earthquakes as an individual scenario from the timelines are further compared under the final earthquake hazard scenario from each timeline.

7.1 | Results and discussion for the high-rise buildings under IH scenario

The 20- and 25-storey base-isolated high-rise RC buildings are analyzed under ten design level earthquakes that correspond to 100-year return period at Nagoya city and six design level winds to observe the performance of the high-rise buildings. The intensity of the earthquakes here used in IH scenario is different from the earthquake events generated in the timeline. The individual earthquakes are made spectrum-compatible with the design spectrum of Nagoya region for return period of 100 years, which is the assumed design life of the base-isolated buildings. The historical earthquakes for phase spectrum are selected from Table 6, which include Sl. No. 2-4, 6-10, 12, and 14. The details of the winds are presented in Table 8. The wind loads are applied on the high-rise buildings based on the distribution of height.

Figure 9 shows the peak response values for top floor displacement, top floor acceleration, cumulative energy dissipation of the isolator, and interstorey drift ratio for the 20- and 25-storey base-isolated high-rise RC buildings under ten individual

TABLE 8 Details of the winds used in this subsection

Sl. No.	Mean speed, U_{10} (m/s)	Duration (min)	Standard deviation (m/s)	Other parameters
1.	25.41	115	6.755	Cut-off frequency: 5 Hz
2.	16.67	111	6.062	Turbulence length:
3.	28.47	113	7.438	$L_{20} = 152.75$ m
4.	37.12	86	7.116	$L_{25} = 170.78$ m
5.	20.62	109	7.701	
6.	31.11	100	6.845	

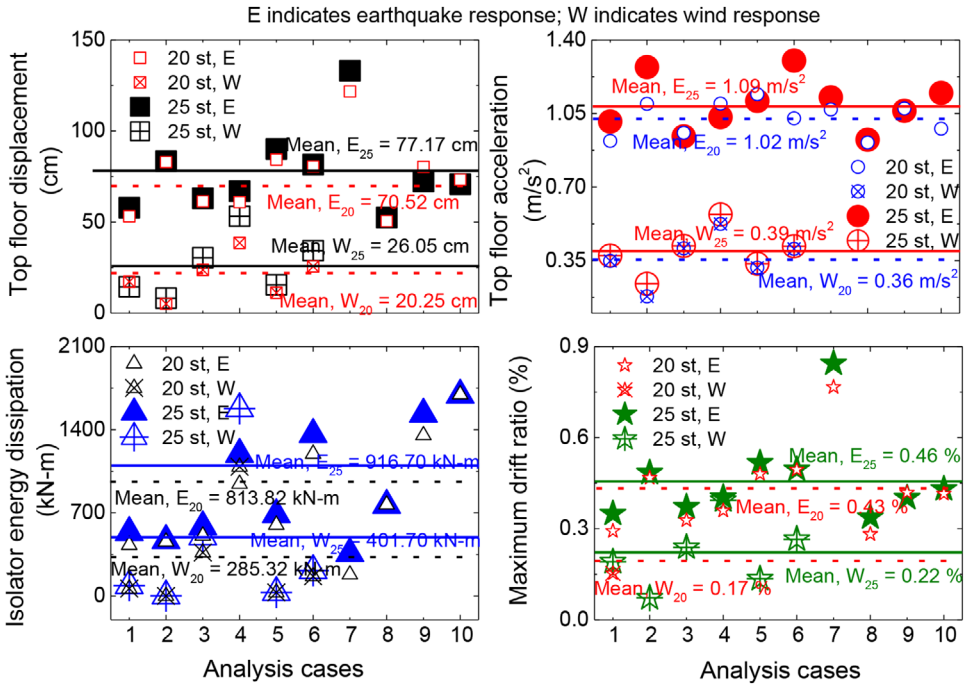

FIGURE 9 Peak response quantities for the 20- and 25-storey base-isolated high-rise reinforced concrete (RC) buildings under individual 10 earthquakes and six winds

earthquakes and six winds. Here, E and W correspond to earthquake and wind events, whereas 20 and 25 indicate the number of storeys considered. The figure also illustrates the difference in the response quantities having a variation of five storeys for the base-isolated high-rise buildings. The mean value of the top floor displacement response for the 20-storey base-isolated high-rise building under the earthquakes is obtained as 70.52 cm, whereas for the 25-storey building, the response is obtained as 77.17 cm. In this case, the percentage difference in the response with such variation in height is observed to be ~9.5%. Similarly, the difference in the mean response under the wind is observed to be ~25%. Moreover, the difference in the mean acceleration response for the 20- and 25-storey under the considered earthquakes and winds are ~6.5% and ~8%, respectively. Hence, the increase in storey for such range of building height has significant contribution for the increase in wind response as compared to the earthquake response.

Figure 9C shows the peak cumulative energy dissipation by the LRBs installed in the 20- and 25-storey high-rise RC buildings. The mean energy dissipation for the LRB in the 20-storey building under the earthquakes is observed to be 813.82 kN m, whereas for the 25-storey building, the same response quantity yields 916.70 kN m under the considered earthquakes. The design values of the LRBs indicate that the size used for the 25-storey building is relatively larger as compared to the 20-storey building; hence, it is obvious that the capacity of the former is relatively greater. However, on observing the energy dissipation per unit volume of the lead core of LRB, it is interesting to see that the unit energy dissipation in the 20-storey high-rise (1.35×10^5 kN m/m^3) is significantly higher as compared to the 25-storey high-rise (1.19×10^5 kN m/m^3) under the earthquakes. However, under the winds, this observation is quite contrary, wherein the unit energy dissipation is significantly higher in the 25-storey building (5.21×10^4 kN m/m^3) as compared to the 20-storey building (4.75×10^4 kN m/m^3). On comparing the mean responses, the energy dissipation for the 25-storey high-rise increases by ~13% under the earthquakes and ~40% under the winds. Moreover, it is interesting to observe that in few selected cases, the peak energy dissipation for the LRBs under the earthquake is almost same as compared to the peak energy dissipation under the wind excitation. For example, the cumulative energy dissipated by the LRB installed in the 20-storey building under the event no. 3, 4, and 7 for the earthquakes and the event no. 3, 4, and 6 for winds is similar in magnitude. The same phenomena can be observed in the 25-storey building, where the LRB dissipates almost similar proportion of energy in the event no. 3, 7, and 9 for the earthquakes and event no. 3, 6, and 4 for the winds. Therefore, the 20- and 25-storey base-isolated high-rise RC buildings can be identified as the type of structures that are governed by the multiple hazard scenarios, wherein the design philosophy needs to be carefully looked into.

Figure 9D shows the maximum interstorey drift ratio of the 20- and 25-storey buildings equipped with the LRBs under the earthquakes and winds. It is also interesting to observe that although the displacement of the 25-storey base-isolated

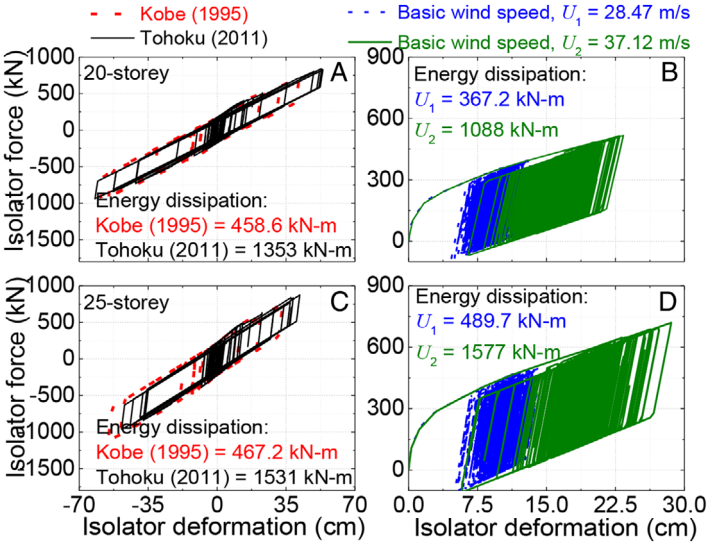

FIGURE 10 Force-deformation of the lead rubber bearings (LRBs) in 20- and 25-storey base-isolated high-rise reinforced concrete (RC) buildings under selected two earthquakes and winds

building is higher under both the hazards, the maximum drift ratio for the 20- and 25-storey buildings under the hazards is almost similar. In this context, it can be reported that the building system designed for earthquake hazard has significant chances to fail under the wind hazard. Hence, it can be concluded that designing the structure resist the large forces under a particular hazard (earthquake) has significant chances to induce similar magnitude of forces under the other hazard (wind), which should be carefully looked into in order to have a safe built environment under the MH scenario.

Figure 10 shows the force-deformation curve for the LRBs equipped in the 20- and 25-storey base-isolated high-rise RC buildings under two selected earthquakes and winds. The spectrum-compatible earthquakes considered here have phase spectrum of Kobe (1995) and Tohoku (2011) earthquakes (refer Table 6: Sl. No. 4 and 10). The wind time history considered here have mean wind speed of 28.47 m/s at 10 m height from the ground and duration of 113 minutes, and mean speed of 37.12 m/s at the same height with 86 minutes duration (refer Table 8: Sl. No. 3 and 4). The cumulative energy dissipation by LRB in the 25-storey high-rise building is significantly more as compared to the 20-storey high-rise under both the earthquakes and winds. Under the earthquakes, the increase in cumulative energy for the 25-storey building is up to ~14%, whereas under the winds, the increase ranges from ~33% to 45%. On close observation, it is noticed that the energy dissipation by LRBs in the 25-storey building under the earthquakes is almost similar in magnitude under the winds. This is attributed to two parameters: isolator deformation amplitude and number of cycles. Under the earthquakes, the isolator deformation amplitude is large; however, the loading occurs for a few several minutes that results in lower number of cycles. On the other hand, the long-duration winds occur for several hours resulting in significantly higher number of cycles, which cause larger energy dissipation despite having relatively lower deformation amplitude. Hence, it is important to recognize the fluctuating component of the wind alongside the duration that results in higher energy dissipation of the energy-dissipating devices. It can be concluded that such kind of structures attract comparable vulnerability under both the hazards. In such cases, the design consideration must be investigated very carefully, as both the dynamic loads contribute to similar proportion of failure in the structure.

Figure 11 illustrates the Fourier amplitude for the 20- and 25-storey base-isolated high-rise RC buildings under the considered earthquake and wind loadings, which demonstrates the frequency content of the response under both the hazards. The figures also illustrate that the earthquake loadings contribute to a wide range of frequency content as compared to the wind loading, which can be observed from the multiple peaks. It is observed that the contribution of multiple modes for the high-rises is significantly higher under the earthquakes as compared to the winds, which have single-mode contribution. Based on modal analysis, the contribution of first mode is more than 82% for both the high-rise buildings. Hence, the approximate post-event period can be determined from the value of the first mode. Here, post-event period indicates the effective period of the base-isolated buildings after completion of the sequential earthquake and wind events. It can also be inferred that the amplitudes under the earthquakes and winds are almost equal, which results in peak response of the structure. Despite additional damaging consequences under the earthquakes, the wind loads also manage to induce significant deformations, which are largely observed in the peak values of the responses.

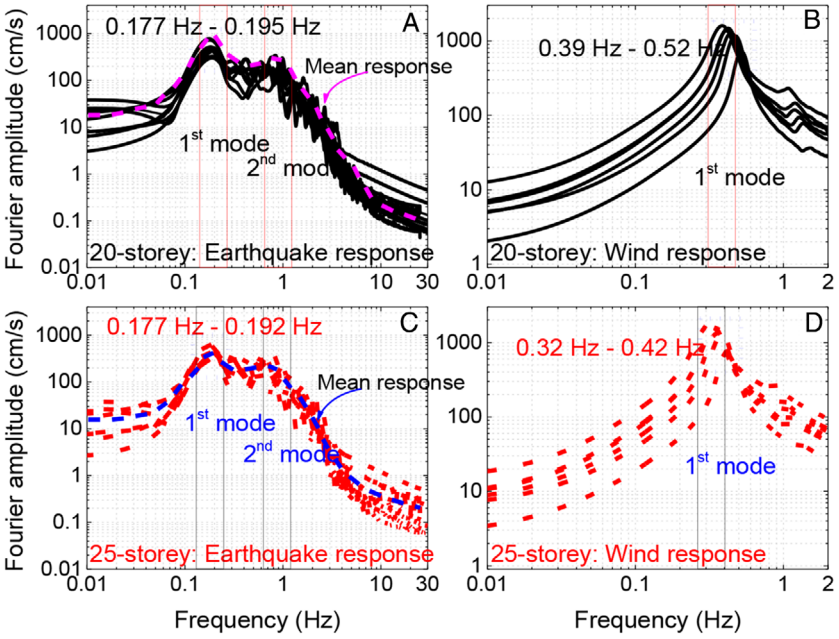

FIGURE 11 Fourier amplitude under the considered 10 earthquakes and six winds

7.2 | Results and discussion for the high-rise buildings under proposed MH scenario

The 20- and 25-storey base-isolated high-rise buildings are further investigated under a sequence of design earthquake and wind loads likely to occur during the lifetime of the buildings. Further, specific cases are studied to understand the performance of the base-isolated buildings considering the effect of the sequence of events (MH) and a single event without any prior damage (IH). For the latter case, the base-isolated high-rise buildings are individually analyzed under earthquakes having phase spectra of three earthquakes corresponding to Sl. No. 91 of Set 1, Sl. No. 90 of Set 4, and Sl. No. 75 of Set 5 (Figure 6). Three design wind loads considered here correspond to Sl. No. 67 of Set 2, Sl. No. 89 of Set 4, and Sl. No. 66 of Set 5. It is to be noted that MH response for this study is observed till the event no. mentioned in the cases, which involves a sequence of analysis considering the degradation of material properties in the previous events. Finally, the responses for the base-isolated high-rise buildings are predicted in terms of displacement and acceleration at isolator level and top floor, and force-deformation relation for the isolator in time and frequency domains.

The periods and mode shapes of the 20- and 25-storey base-isolated high-rise buildings before and after the sequence of MH events are also estimated for design life of the buildings. The fundamental periods for the 20- and 25-storey high-rises are 1.928 and 2.324 seconds, respectively. On the other hand, the fundamental periods for the base-isolated high-rises against five different timeline sets range from 3.037 to 3.647 seconds (20-storey) and from 3.6 to 3.711 seconds (25-storey). The fundamental periods of both the 20- and 25-storey high-rises increase significantly, thereby demonstrating the effect of MH scenario in design life. The change in the fundamental period is attributed to the change in effective stiffness of the LRBs after the events. The fundamental periods for the 20-storey high-rise building increase from ∼55% to ∼90%, whereas the same for the 25-storey high-rise increases from ∼55% to ∼60%. This can be attributed to the damage induced in the LRBs that substantially changed the period of the high-rise buildings. The effect in superstructure is marginal as can be observed in the mode shapes. On comparing the modal period of the base-isolated high-rises under the IH scenario, the increase in the 20- and 25-storey buildings is observed to be up to ∼5%, which is generally neglected in the design for a single-hazard scenario. Hence, the damage in the LRBs needs to be accounted for the vibration of the superstructure of the base-isolated high-rises.

Figures 12 and 13 present the deformation history of the LRB installed in the 20-storey high-rise building under three earthquakes and winds mentioned above. Under the earthquakes and winds, the behavior of the 20-storey building under the sequence of the loadings (MH) is different from the IH analysis, as observed from the waveforms of isolator displacement. The effective stiffness decreases substantially under the MH event, thereby allowing more deformation of the LRBs. The displacement waveforms indicate that the 20-storey building experiencing MH scenario has induced damage to the LRBs, which in turn increases the fundamental period of the building. Further, the LRBs are observed to have strong restoring force-deformation characteristics under the IH as well as MH analysis under the earthquakes, although the MH

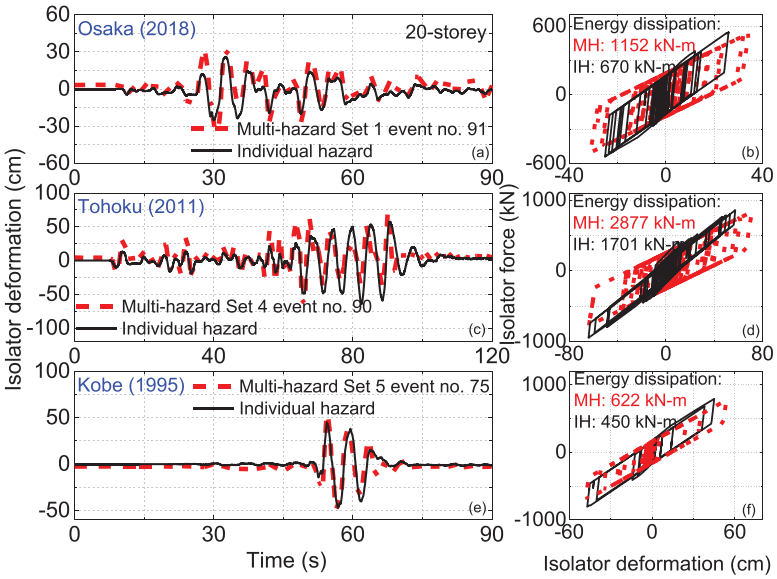

FIGURE 12 Isolator response of 20-storey building for seismic loadings under the individual and multihazard scenarios

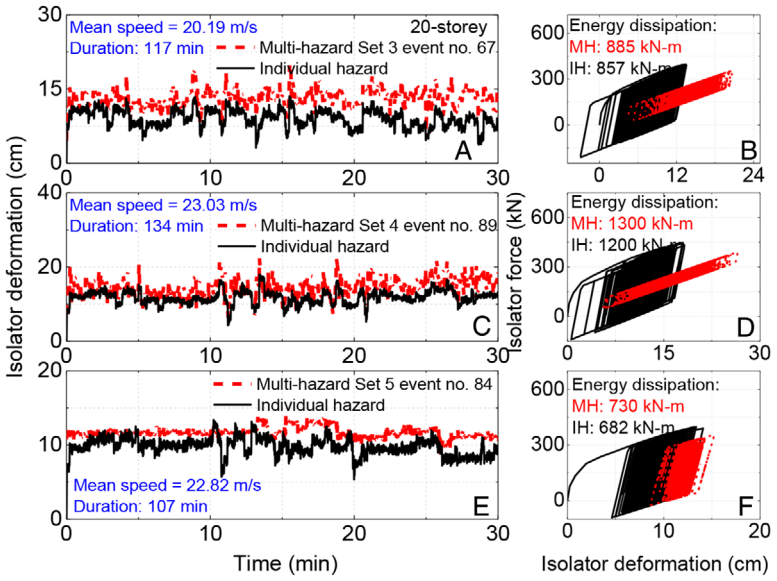

FIGURE 13 Isolator response of 20-storey building for wind loadings under the individual and multihazard scenarios

event induces slight residual deformation (up to 1.7 cm) due to strength degradation property of the LRBs. The cumulative energy dissipation, represented by the force-deformation curve, shows that the energy dissipated by the LRBs under the MH scenario is significantly higher as compared to the energy dissipated under the individual earthquakes. In this case, the energy dissipation under the MH event increases from ~38% to 72%. On the other hand, the deformation of the LRBs under the winds increases significantly, whereas the strength of the LRBs has substantial decrease. It is interesting to observe that the force-deformation curves for IH and MH events for wind speed 22.82 m/s have similar effective stiffness. This is due to less number of earthquakes in design life as compared to the other sets that induces lesser force until that event. Finally, the energy dissipation under the MH scenario is slightly higher as compared to the individual wind scenarios, which is up to ~8.5%.

Figure 14 deals with the isolator displacement response of the 20- and 25-storey base-isolated buildings in frequency domain under the three earthquake and wind scenarios considered above. The sequence of events generated in design life of the buildings has inflicted significant damage to the LRBs, as observed from the shift in frequency at peak amplitude. The effect is more prominent under the wind loads. The long-duration nature induces large number of cycles that help in significant energy dissipation, which in turn causes degradation in strength and stiffness of the LRBs. Although, the response history in time domain (Figures 12 and 13) under the earthquakes for the MH scenario shows significant residual deformation in the LRBs, the frequency content of the MH response has marginal difference as compared to the IH

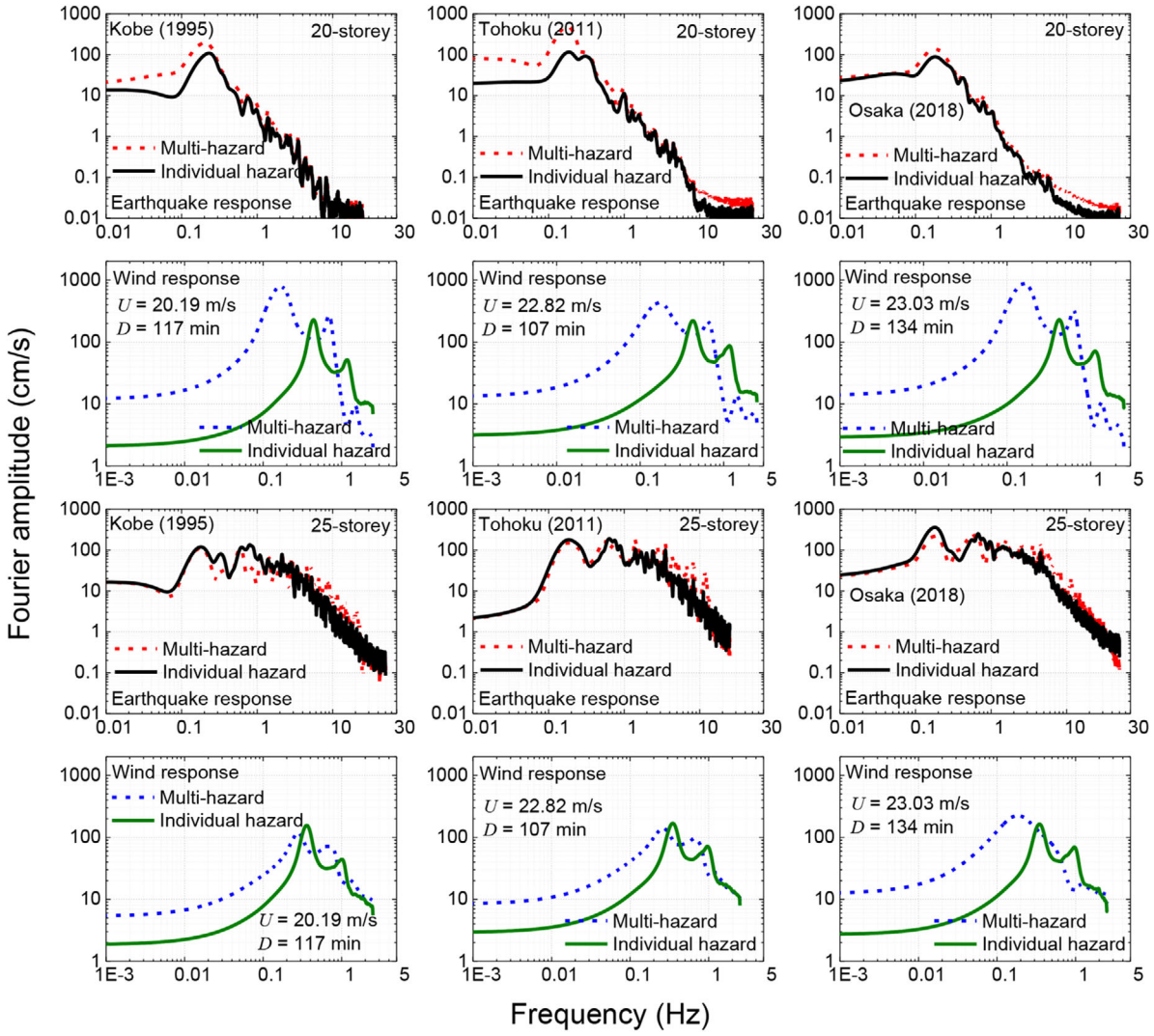

FIGURE 14 Fourier amplitude of isolator displacement response under individual and multihazard scenarios

response. Therefore, the responses in frequency domain help to understand the nature of the responses, which generally are not depicted in case of the time domain results.

7.3 | Fatigue behavior of the LRBs using the proposed MH methodology

In addition to the traditional response parameters discussed above, the fatigue behavior of the LRBs in the 20- and 25-storey base-isolated high-rise RC buildings are also investigated under the MH scenario of earthquakes and winds. The fatigue performance of the LRBs is characterized by developing fatigue curve that determines the threshold limit of fatigue for the considered isolation devices. Figure 15 indicates the number of cycles and the corresponding deformation amplitude of the LRBs in 20- and 25-storey base-isolated high-rise buildings under the generated MH timeline as well as under individual earthquake and wind hazards. The fatigue responses of both the LRBs significantly exceed the limiting criteria under the sequence of earthquake and wind hazards for two sets of events, indicating a concern for the safety of the base-isolated high-rise buildings. Although the deformation amplitude under the MH events is marginally lower as compared to the individual earthquake events, the increase in the number of cycles tend to dissipate larger amount of energy, thereby contributing to the failure of the device. Hence, it may be concluded that the existing design philosophy in which either of the maximum of earthquake or wind load is utilized, may have high chance to underestimate the distress

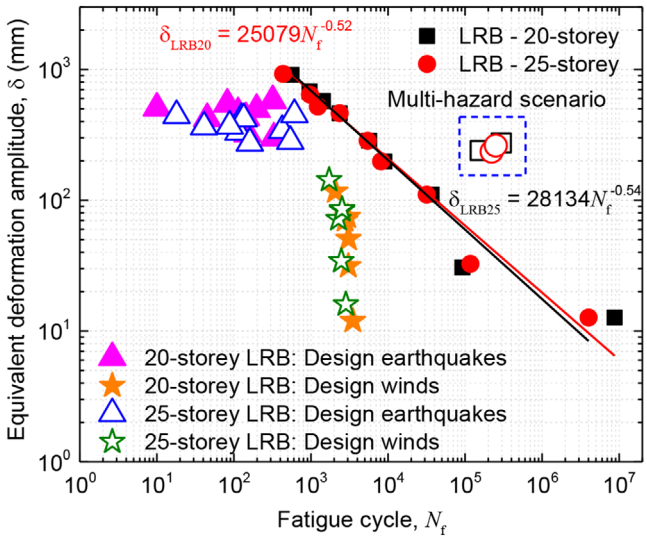

FIGURE 15 Fatigue curve for the lead rubber bearings (LRBs) indicating fatigue response

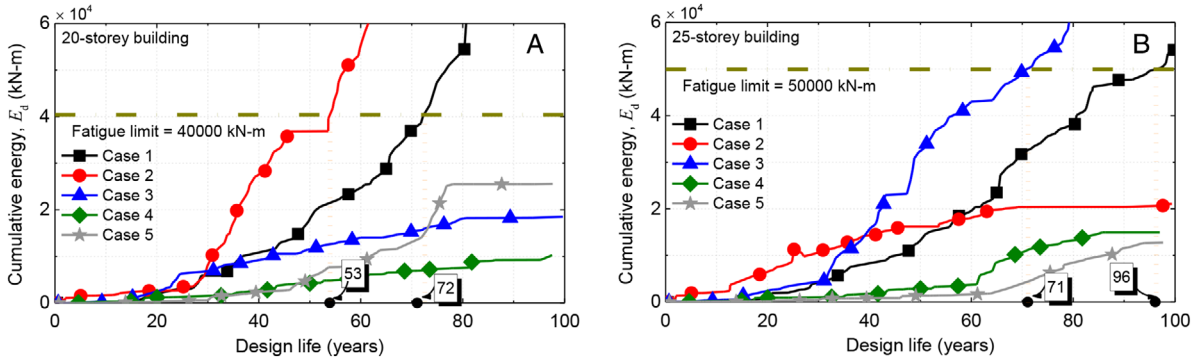

FIGURE 16 (A) Fatigue life of the LRB installed in the 20-storey high-rise building. (B) Fatigue life of the lead rubber bearing (LRB) installed in the 25-storey high-rise building

level occurring in the isolation devices, especially the LRBs. Hence, such critical concern calls for development of more advanced methodology to assess and design structures under multiple earthquake and wind scenarios.

Figures 16A and 16B present the cumulative energy accumulation in the LRBs of the 20- and 25-storey high-rise buildings under the sequence of multiple earthquakes and winds likely to occur in design life of the buildings. For both the base-isolated high-rise buildings, the cumulative energy in two cases are observed to exceed the threshold capacity of the LRBs, which is 4×10^4 kN m for the 20-storey and 5×10^4 kN m for the 25-storey base-isolated buildings. It is also interesting to observe that the LRBs lose their energy-dissipating capacity in no lesser than ~53 years for the 20-storey, and ~71 years for the 25-storey high-rises, which solely depends on the occurrence rates of the natural hazards. Thus, the fatigue life of the LRBs are 53 years for the 20-storey and ~71 years for the 25-storey base-isolated high-rises, which mandates the stakeholders to address the MH issue in due course of time. Therefore, the MH effect should be emphasized relatively more in region with higher occurrence of multiple hazards such as earthquakes and winds, as such scenarios have the serious potential to inflict sufficient damage in design life, despite the structure being designed with any passive control devices.

8 | CONCLUSIONS

To conclude, a methodology is derived and proposed for generating a timeline of earthquake and wind events during design life of a structure. The proposed methodology is used to investigate the performance of 20- and 25-storey base-isolated high-rise RC buildings. The base-isolated high-rises are investigated under a set of individual design

earthquakes and winds, which are compared against the results obtained using the proposed methodology. The responses for the base-isolated high-rise buildings are predicted in terms of displacement and acceleration at isolator level and top floor, and force-deformation relation at the isolator level. The fatigue performance of the LRBs is estimated by developing fatigue curves, and the fatigue life of the LRBs is determined under the developed MH scenario. The developed methodology can be used in other regions, based on the occurrence of earthquake and wind events for the design period. Hence, in context of this research conducted, the major conclusions drawn are as follows:

1. The 20- and 25-storey base-isolated high-rise RC buildings are identified to be governed by multiple hazard scenarios, wherein the building systems designed to resist the earthquake load tend to be vulnerable under the wind load. Therefore, it is recommended that design of such building types should include the effects of both the hazards.
2. The existing design philosophy, where either of the maximum of earthquake or wind load is utilized, has high chance to underestimate the distress level occurring in the isolation devices wherein the installed passive devices may undergo fatigue failure, thus questioning the global safety of the structure.
3. The MH scenario in design life induces change in the fundamental period of the base-isolated high-rise buildings without allowing damage in the superstructure, which is mainly due to the damage in the isolation systems. Hence, the damage in the LRBs needs to be accounted for the vibration of the superstructure of the base-isolated high-rises.
4. It is extremely crucial to consider the fluctuating component of the wind along with the duration for designing of structures against wind. Therefore, low-amplitude high-cycle excitations are of significant concern for long-term responses, such as fatigue behavior of energy-dissipating devices, wherein the common design parameters are not affected generally.
5. The frequency content as well the frequency range at peak amplitudes of the induced response indicate that non-structural elements having low frequency are extremely vulnerable under the considered ground motion and wind scenarios.
6. The fatigue life of the LRBs are 53 years for the 20-storey and ~71 years for the 25-storey base-isolated high-rises that were investigated in this study, which mandates the stakeholders to address the MH issue in due course of time.

ACKNOWLEDGMENTS

The authors sincerely thank Suzuki Foundation for providing this opportunity to carry out this collaborative academic research at Toyohashi University of Technology (TUT), Japan. The collaborative work being reported here is facilitated by a memorandum of understanding between Indian Institute of Technology (IIT) Delhi and TUT for academic cooperation. The opinions expressed herein are those of the authors and not necessarily of the funding agencies.

DATA AVAILABILITY STATEMENT

All data, models, and code generated or used during the study appear in the submitted article.

ORCID

Tathagata Roy https://orcid.org/0000-0002-7238-8142
Taiki Saito https://orcid.org/0000-0002-4249-119X
Vasant Matsagar https://orcid.org/0000-0002-7600-0520

REFERENCES

1. Tezuka T, Hirashima S. Evaluation of total seismic cost for long life structural system. *AIJ J Technol Des*. 2000;6(10):67-70.
2. Matsagar VA, Jangid RS. Influence of isolator characteristics on the response of base-isolated structures. *Eng Struct*. 2004;26(12):1735-1749.
3. Omiya M, Kitamura H. Investigation and analysis on the structural characteristics of the recent base isolated buildings corresponding to long-period ground motion. *AIJ J Technol Des*. 2019;25(59):61-66.
4. Kodakkal A, Saha SK, Sepahvand K, Matsagar VA, Duddeck F, Marburg S. Uncertainties in dynamic response of buildings with non-linear base-isolators. *Eng Struct*. 2019;197:109423.
5. Stanikzai MH, Elias S, Matsagar VA, Jain AK. Seismic response control of base-isolated buildings using tuned mass damper. *Aust J Struct Eng*. 2020;21(1):310-321.
6. Katagiri J, Ohkuma T, Yasui H, Marukawa H, Tsurumi T. Study of accuracy for reduced model of high-rise buildings with base isolation. *AIJ J Technol Des*. 2012;17(36):461-466.
7. Feng C, Chen X. Estimation of inelastic crosswind response of base-isolated tall buildings: performance of statistical linearization approaches. *ASCE J Struct Eng*. 2019;145(12):04019161.
8. Liang B, Shishu X, Jiaxiang T. Wind effects on habitability of base-isolated buildings. *J Wind Eng Ind Aerodyn*. 2002;90(12-15):1951-1958.

9. Chimamphant S, Kasai K. Comparative response and performance of base-isolated and fixed-base structures. *Earthq Eng Struct Dyn*. 2016;45(1):5-27.
10. Hayashi Y, Murase S, Sugino M. Super high-rise buildings in Osaka prefecture. *AIJ J Technol Des*. 2018;24(58):1075-1078.
11. Becker TC, Yamamoto S, Hamaguchi H, Higashino M, Nakashima M. Application of isolation to high-rise buildings: a Japanese design case study through a U.S. design code lens. *Earthq Spectra*. 2019;31(3):1451-1470.
12. Ariga T, Kanno Y, Takewaki I. Resonant behavior of base-isolated high-rise buildings under long-period ground motions. *Struct Des Tall Special Build*. 2006;15(3):325-338.
13. Roussis PC, Constantinou MC. Uplift-restraining friction pendulum seismic isolation system. *Earthq Eng Struct Dyn*. 2006;35(5):577-593.
14. Takewaki I. Robustness of base-isolated high-rise buildings under code-specified ground motions. *Struct Des Tall Special Build*. 2008;17(2):257-271.
15. Ma CF, Zhang YH, Tan P, Zhou FL. Seismic response of base-isolated high-rise buildings under fully nonstationary excitation. *Shock Vib*. 2014;2014:401469.
16. Nakai A, Sato D, Murakami T, Kasai K. Evaluation of stiffness of base-isolation layer and superstructure of high-rise base-isolated building based on seismic observation recording. *AIJ J Technol Des*. 2018;24(57):571-576.
17. Lu X, Wang D, Wang S. Investigation of the seismic response of high-rise buildings supported on tension-resistant elastomeric isolation bearings. *Earthq Eng Struct Dyn*. 2016;45(13):2207-2228.
18. Zhang W, Yin X, Chen Y, Fei K. Seismic performance of high-rise building with a rock-slip isolation system with cables. *Struct Des Tall Special Build*. 2020;29(4):e1705.
19. Feng C, Chen X. Evaluation and characterization of probabilistic along-wind and crosswind responses of base-isolated tall buildings. *J Eng Mech*. 2019;145(12):04019097.
20. Kareem A. Modelling of base-isolated buildings with passive dampers under winds. *J Wind Eng Ind Aerodyn*. 1997;72(1-3):323-333.
21. Kouchiyama O, Ikenaga M, Nakamura T, et al. *Study on LRB Performance of High-Rise Base-Isolated Building During Strong Wind*. 13th World Conference on Earthquake Engineering (13WCEE), Vancouver, British Columbia (BC), Canada; 2004.
22. Yasui H, Ohkuma T, Marukawa H. Study on wind response characteristics of base-isolated buildings with creep. *J Struct Constr Eng*. 2007;72(619):41-48.
23. Higashino M, Ohtake K, Hamaguchi H, Wada A. Durability of sliding isolation device employed in super high-rise buildings subjected to wind excitations. *J Struct Constr Eng*. 2010;75(648):317-325.
24. Katagiri J, Ohkumab T, Marukawaa H, Yasui H. Unstable aerodynamic responses of base-isolated high-rise buildings. *J Struct Constr Eng*. 2012;77(681):1637-1644.
25. Li Z, Huang G, Chen X, Zhou Y, Yang Q. Wind-resistant design and equivalent static wind load of base-isolated tall building: a case study. *Eng Struct*. 2020;212:110533.
26. JSSI. *Guidelines for the Wind-Resistant Design of Seismically Base-Isolated Buildings*. The Japan Society of Seismic Isolation; 2017;1-126.
27. Roy T, Matsagar V. Effectiveness of passive response control devices in buildings under earthquake and wind during design life. *Struct Infrastruct Eng*. 2019;15(2):252-268.
28. Roy T, Matsagar V. Probabilistic assessment of steel buildings installed with passive control devices under multihazard scenario of earthquake and wind. *Struct Saf*. 2020;85:101955.
29. Susilo D, Indrasari M, Harliantaraa JI, Yunus E. Managing uncertainty during disaster: case on typhoon Hagibis Japan. *IOP Conf Ser: Earth Environ Sci*. 2020;519(1):012015.
30. Holmes JD. Fatigue life under along-wind loading - closed-form solutions. *Eng Struct*. 2002;24:109-114.
31. MLIT. *The Notification and Commentary on the Structural Calculation Procedures for Building with Seismic Isolation* (in Japanese). Japan: Ministry of Land, Infrastructure, Transport and Tourism; 2000.
32. JSSI. *Design Guideline of Seismically Isolated Building by Time History Response Analysis*. The Japan Society of Seismic Isolation; 2018.
33. Bridgestone Corporation. http://www.bridgestone.com/products/diversified/antiseismic_rubber/index.html. Accessed November 28, 2020.
34. Saito T. *STructural Earthquake Response Analysis 3D Version 10.3 (STERA_3D v10.3)*. 2019. http://www.rc.ace.tut.ac.jp/saito/software-e.html. Accessed November 28, 2020.
35. Kalpakidis IV, Constantinou MC. Effects of heating on the behavior of lead-rubber bearings. I: Theory. *ASCE J Struct Eng*. 2009;135(12):1440-1449.
36. Kalpakidis IV, Constantinou MC. Effects of heating on the behavior of lead-rubber bearings. II: Verification of theory. *ASCE J Struct Eng*. 2009;135(12):1450-1461.
37. Kalpakidis IV, Constantinou MC. Principles of scaling and similarity for testing of lead-rubber bearings. *Earthq Eng Struct Dyn*. 2010;39(13):1551-1568.
38. Kalpakidis IV, Constantinou MC, Whittaker AS. Modeling strength degradation in lead-rubber bearings under earthquake shaking. *Earthq Eng Struct Dyn*. 2010;39(13):1533-1549.
39. Kalpakidis IV, Constantinou MC, Whittaker AS. Effects of large cumulative travel on the behavior of lead-rubber seismic isolation bearings. *ASCE J Struct Eng*. 2010;136(5):491-501.
40. Takaoka E, Takenaka Y, Kondo A, et al. Long-duration loading test on lead rubber bearings considering wind load. *AIJ J Technol Des*. 2012;18(38):61-66.

41. Kouchiyama O, Kanda T, Takenaka Y, Miyazaki M, Nakamura M, Kitamura H. Experimental study on fatigue characteristics of lead rubber bearings under repeated small-amplitude loading. *AIJ J Technol Des*. 2015;21(48):639-644.
42. Kumar M, Whittaker AS, Constantinou MC. An advanced numerical model of elastomeric seismic isolation bearings. *Earthq Eng Struct Dyn*. 2014;43(13):1955-1974.
43. Shinohara S, Hoshikuma J. Experimental study on characteristic evaluation of laminated rubber bearings with lead plugs damaged by earthquake [In Japanese]. *J Jpn Soc Civ Eng Ser A1*. 2015;71(4):I_587-I_599.
44. Dang J, Higashide T, Igarashi A, Adachi Y, Hayashi T. Dynamic analysis to investigate the effect of aging deterioration of lead rubber bearings on the seismic performance of bridges [In Japanese]. *J Jpn Soc Civ Eng Ser A1*. 2015;71(4):I_713-I_724.
45. Hayashi K, Adachi Y, Komoto K, et al. Experimental verification of the remaining performance of the aging the lead plug rubber bearing [In Japanese]. *J Jpn Soc Civ Eng Ser A1*. 2014;70(4):I_1032-I_1042.
46. Constantinou M, Tsopelas P, Kasalanati A, Wolff E. *Property Modification Factors for Seismic Isolation Bearings*. Buffalo, NY: Multidisciplinary Center for Earthquake Engineering Research; 1999.
47. Baker JW. Conditional mean spectrum: tool for ground motion selection. *ASCE J Struct Eng*. 2011;137(3):322-331.
48. Atkinson GM, Davenport AG, Novak M. Seismic risk to pipelines with application to Northern Canada. *Can J Civ Eng*. 1982;9:248-264.
49. Erel B, Patelunas GM, Niece JE, Oppenheim IJ. Measuring the earthquake performance of urban water systems. In: *Current State of Knowledge of Lifeline Earthquake Engineering*. Vol 103. American Society of Civil Engineers; 1977:183-198.
50. Cornell CA, Merz HA. Seismic risk analysis of Boston. *ASCE J Struct Eng*. 1975;101:2027-2041.
51. Kiureghian AD, Ang AHS. A fault-rupture model for seismic risk analysis. *Bull Seismol Soc Am*. 1977;671:173-1194.
52. AIJ. *Recommendations for Loads on Buildings*. Architectural Institute of Japan; 2015.
53. Zhang X, Yan W, He H, Sun Y, Chen S. Generation of uniform hazard spectrum based on the stochastic method of simulating ground motion and its use in nuclear power plants. *Adv Civil Eng*. 2018;2018:6037863.
54. Pandey MD, van der Weide H. Probability distribution of the seismic damage cost over the life cycle of structures. *Struct Saf*. 2018;72:74-83.
55. Baker JW. *Introduction to Probabilistic Seismic Hazard Analysis*. White Paper Version 2.1; 2015:1-77.
56. Kiureghian AD. Non-ergodicity and PEER's framework formula. *Earthq Eng Struct Dyn*. 2005;34(13):1643-1652.
57. Gutenberg B, Richter CF. *Seismicity of the Earth and Associated Phenomena*. Princeton, NJ: Princeton University Press; 1954.
58. Goda K, Taylor CA. Effects of aftershocks on peak ductility demand due to strong ground motion records from shallow crustal earthquakes. *Earthq Eng Struct Dyn*. 2012;41(15):2311-2330.
59. Mukherjee S, Gupta VK. Wavelet-based generation of spectrum-compatible time-histories. *Soil Dyn Earthq Eng*. 2002;22(9):799-804.
60. Ni S-H, Xie W-C, Pandey MD. Generation of spectrum-compatible earthquake ground motions considering intrinsic spectral variability using Hilbert-Huang transform. *Struct Saf*. 2013;42:45-53.
61. Saito T. *STructural Earthquake Response Analysis WAVE version 1.0 (STERA_WAVE)*. 2019. http://www.rc.ace.tut.ac.jp/saito/software-e.html. Accessed November 28, 2020.
62. Jennings PC, Housner GW, Tsai NC. *Simulated Earthquake Motions for Design Purpose*. Proceedings of 4th World Conference on Earthquake Engineering; 1969;145-160.
63. Japan Meteorological Agency (JMA). https://www.jma.go.jp/jma/indexe.html. Accessed November 19, 2020.
64. Wang J, Cheynet E, Snæbjörnsson JÞ, Jakobsen JB. Coupled aerodynamic and hydrodynamic response of a long span bridge suspended from floating towers. *Wind Eng Ind Aerodyn*. 2018;177:19-31.
65. Deodatis G, Shinozuka M. Weighted integral method. II: Response variability and reliability. *ASCE J Eng Mech*. 1991;117(8):1865-1877.
66. Deodatis G. Simulation of ergodic multivariate stochastic processes. *ASCE J Eng Mech*. 1996;122(8):778-787.
67. Jiao Y, Kishiki S, Yamada S, et al. Low cyclic fatigue and hysteretic behavior of U-shaped steel dampers for seismically isolated buildings. *Earthq Eng Struct Dyn*. 2015;44(10):1523-1538.
68. JSSI. Report of investigation committee on response control buildings. *The Japan Society of Seismic Isolation*; 2012.

How to cite this article: Roy T, Saito T, Matsagar V. Multihazard framework for investigating high-rise base-isolated buildings under earthquakes and long-duration winds. *Earthquake Engng Struct Dyn*. 2021;50:1334–1357. https://doi.org/10.1002/eqe.3401